VII International Conference on Computational Methods in Marine Engineering
MARINE 2017
M. Visonneau, P. Queutey and D. Le Touzé (Eds)

A GENERALISED UNSTEADY HYBRID DES/BEM METHODOLOGY APPLIED TO PROPELLER-RUDDER FLOW SIMULATION

D. CALCAGNI*[1], F. SALVATORE*, G. DUBBIOSO*, R. MUSCARI*

* Marine Technology Research Institute
National Research Council (CNR-INSEAN)
Via di Vallerano, 139, 00128 Rome, Italy
[1]e-mail: danilo.calcagni@cnr.it, web page: http://www.insean.cnr.it/

Key words: Propulsion, CFD, Hybrid DES/BEM, propeller-rudder interaction

Abstract. A generalised hybrid viscous/inviscid flow model for the hydrodynamic analysis of marine propellers is presented. A Boundary Element Method (BEM) to predict propeller perturbation under inviscid-flow assumptions is combined with a Navier-Stokes solver to describe the viscous, turbulent flow with propeller effects recast as volume-force terms from BEM. In the present study, the viscous flow solution is based on a Detached Eddy Simulation (DES) model valid for unsteady flows. A numerical application is presented by considering a notional propeller-rudder assembly, and results from the hybrid DES/BEM solution are validated by comparisons with full DES. The validation study demonstrates the capability of the proposed hybrid viscous/inviscid flow model to describe transient propeller-induced flow perturbation and of propeller/rudder interaction in spite of the fact that the geometry of propeller blades is not resolved but described via a simple and fast volume force model.

1 INTRODUCTION

Computational Fluid Dynamics (CFD) tools based on the numerical solution of the Navier-Stokes equations have proven the capability to correctly simulate the complex flow features that characterize the interaction of a rotating propeller with the ship hull and its appendages.

The detailed analysis of the propeller-rudder assembly deserves a specific attention in many applications. Ship manoeuvring simulations require a careful prediction of rudder loads averaged over the propeller revolution period with transient flow effects limited to describe the non-uniform inflow to the propeller. Transient loads induced on the rudder surface by propeller swirled flow and trailing vorticity become important to identify the occurrence of eccessive pressure pulses on the rudder surface with related risks for erosive cavitation, vibrations, noise radiation. The global cost of a time-accurate analysis by CFD with resolved rotating propellers is very high both in terms of mesh generation and computing time of time-marching solutions with very small time scales associated to propeller rotational speed.

Classical actuator disk approaches, *e.g.* [18], that are used to limit the computational burden of viscous flow simulations around a fully appended hull can only describe averaged propeller effects and hence cannot be used in problems where transient flow perturbations are of interest. An evolution of actuator disk models is represented by the so-called hybrid viscous/inviscid models in which lifting-line, vortex-lattice [5] [20], Boundary Element Methods (BEM, [4] [12] [16]) solvers to predict propeller induction are combined with Reynolds-Averaged Navier-Stokes Equation (RANSE) solvers to describe the viscous turbulent flow around ship hull and appendages. In spite of more generality with respect to actuator disk models, in most cases the coupling between RANSE and propeller model is limited to steady flow conditions.

Few attempts have been made to fully generalise the approach in order to describe the transient flow perturbation induced by the propeller. Examples are [19], in which the unsteady flow around a podded propeller with ventilation effects is investigated by a hybrid RANSE/BEM model, and [15] in which the transient flow around an isolated propeller in uniform flow is studied by hybrid RANSE/BEM and results are validated by comparing with fully unsteady RANSE.

Aim of the present paper is to follow-up the work in [1], [15] and use the same unsteady viscous/inviscid coupling strategy with RANSE solver replaced by a Detached Eddy Simulation (DES) solver to better describe transient flow features in the propeller wakefield. To the authors' knowledge this is the first case of a hybrid viscous/inviscid model for ship hydrodynamics in which a DES solver is used. The viscous flow solver is the χ-Navis code, the propeller flow model is the BEM solver PRO-INS, both developed at CNR-INSEAN, see *e.g.* [3] and [14]. The coupling of the PRO-INS solver with a different RANSE solver is described in [2].

A numerical application of the proposed hybrid DES/BEM model is presented by considering a notional propeller-rudder assembly given by an infinite-span straigth rudder placed in the race of the INSEAN E779A model propeller [13]. Numerical results include transient loads on both propeller and rudder, velocity distributions and pressure distributions on the rudder. Predictions by the hybrid model are compared with results by full DES [11] to analyse the capability of the proposed DES/BEM coupling to reproduce transient flow features characterizing the interaction between propeller and rudder.

2 THEORETICAL AND COMPUTATIONAL MODEL

The proposed hybrid viscous/inviscid model extends a formulation presented in [15] in which the velocity field is assumed to be the combination of two contributions: an arbitrary onset flow with velocity $\mathbf{w}$ and the velocity perturbation $\mathbf{v}_P$ induced by a propeller immersed in it. Propeller flow is studied by a boundary element model for inviscid flows, while a Navier-Stokes solver is used to describe the onset flow under general viscous flow conditions.

A Reynolds-Averaged Navier-Stokes model is considered in [15], whereas Detached Eddy Simulation (DES) is addressed here. The boundary integral formulation for inviscid flows is valid for an isolated propeller in unbounded flow. Propeller-rudder interaction is described through the coupling between propeller flow and onset flow problems, as explained later.

2.1 Inviscid flow model by BEM

Assuming an inviscid, irrotational propeller-induced flow, perturbation velocity can be described in terms of a scalar velocity potential, $\mathbf{v}_P = \nabla\varphi$. Under incompressible flow assumptions,

mass and momentum equations yield that the velocity potential φ satisfies the Laplace equation and the pressure p follows from the Bernoulli equation, respectively

$$\nabla^2\varphi = 0, \qquad \frac{\partial\varphi}{\partial t} + \frac{1}{2}\|\nabla\varphi + \mathbf{v}_I\| + \frac{p}{\rho} + gz_0 = \frac{1}{2}\|\mathbf{v}_I\|^2 + \frac{p_0}{\rho}, \tag{1}$$

where ρ is water density, p_0 is the free-stream reference pressure and gz_0 is the hydrostatic head. Quantity $\mathbf{v}_I = \mathbf{w} + \boldsymbol{\Omega} \times \mathbf{x}$ denotes the inflow to the propeller as observed from a frame of reference $(Ox_F y_F z_F)$ (Fig. 1(a)) fixed with the propeller rotating at angular velocity $\boldsymbol{\Omega}$, while $\mathbf{w}$ is the onset flow velocity, to be studied under viscous-flow assumptions, as described later.

Boundary conditions for φ are obtained by imposing vanishing perturbation at infinity and impermeability on the propeller surface, that is $(\mathbf{v}_P + \mathbf{v}_I) \cdot \mathbf{n} = 0$, or

$$\frac{\partial\varphi}{\partial n} = -(\mathbf{w} + \boldsymbol{\Omega} \times \mathbf{x}) \cdot \mathbf{n} \tag{2}$$

where $\mathbf{n}$ is the unit normal to the surface. Potential flow theory applied to lifting bodies implies the introduction of a potential-discontinuity surface, the trailing wake $\mathcal{S}_W$, where vorticity generated on blades is shed downstream. An analytical helicoidal wake surface model is used here.

Following [7], the Laplace equation for φ is solved by a boundary integral representation as

$$E(\mathbf{x})\,\varphi(\mathbf{x},t) = \int_{\mathcal{S}_B} \left(\frac{\partial\varphi}{\partial n}G - \varphi\frac{\partial G}{\partial n}\right) d\mathcal{S} - \int_{\mathcal{S}_W} \Delta\varphi_{TE}(t-\tau)\frac{\partial G}{\partial n} d\mathcal{S} \tag{3}$$

where $\mathcal{S}_B$ is the propeller surface, t is time, $\Delta\varphi_{TE}$ denotes potential discontinuity at blade trailing edge where the wake is shed and τ is the shedding delay associated to wake points (Kutta condition). Quantities $G, \partial G/\partial n$ are unit source and dipole in the unbounded three-dimensional space, and $E(\mathbf{x})$ is a field function to distinguish the case where $\mathbf{x}$ is inside the flow field ($E = 1$) or on the solid boundary surface ($E = 1/2$).

Recalling $\mathbf{v}_P = \nabla\varphi$ and Eq. (2), propeller induced velocity may be evaluated from Eq. (3) through a linear problem in which unknowns are located on the propeller surface.

The numerical solution of Eq. (3) is obtained here by a low-order Boundary Element Method implemented into the PRO-INS code developed by CNR-INSEAN. Once φ on $\mathcal{S}_B$ is known, the pressure p is determined from the Bernoulli theorem, and hydrodynamic forces acting on propeller blades follow as

$$\mathbf{f} = \sum_{n=1}^{Z} \int_{\mathcal{S}_{B_n}} (-p\mathbf{n} + \boldsymbol{\tau})\, d\mathcal{S}, \tag{4}$$

where $\mathcal{S}_{B_n}$ $(n = 1, \ldots Z)$ denotes the surface of the n-th blade of a Z–bladed screw. Using a common approach in inviscid-flow models, the distribution of viscosity–induced tangential stress $\boldsymbol{\tau}$ is estimated by using expressions that are valid for flat plates in laminar and turbulent flow at same Reynolds number as blade sections.

2.2 Viscous flow model by DES

The viscous flow surrounding the propeller is evaluated by integration of the Navier-Stokes equations for unsteady incompressible flows:

$$\begin{aligned} \nabla \cdot \mathbf{v} &= 0 \\ \frac{\partial \mathbf{v}}{\partial t} + (\mathbf{v} \cdot \nabla)\mathbf{v} &= -\frac{1}{\rho}\nabla p + \nu \nabla^2 \mathbf{v} + \mathbf{B} \end{aligned} \tag{5}$$

where quantity $\mathbf{B}$ denotes a generic source term. In the present work, it represents the propeller induced forces predicted by BEM.

The numerical algorithm to solve Eq. (5) is implemented into an in–house solver based on a finite volume technique with pressure and velocity co-located at cell center. Viscous terms are integrated by a standard second order centered scheme, whereas for the convective and pressure terms a third order upwind scheme is chosen. Of course, because of the treatment of the viscous terms, the scheme remains formally second order in space. The turbulence closure is based on the Detached Eddy Simulation (DES) version of the Spalart-Allmaras turbulence model [17].

The physical time derivative in the governing equations is approximated by a second-order accurate, three-point backward finite difference formula [3]. In order to obtain a divergence free velocity field at every physical-time step, a pseudo-time derivative is introduced in the discrete system of equations [6]. As it will be explained in the following, every n pseudo-time steps of the inner iteration (n being a parameter chosen through numerical tests) the BEM algorithm is invoked in order to update the $\mathbf{B}$ term in Eq. (5).

No-slip boundary conditions are enforced at solid walls. At the inlet boundary the velocity is set to the undisturbed flow value, whereas at the outflow the pressure is set equal to zero.

The mesh built to discretize the fluid domain is composed by structured, partially overlapping blocks, and a chimera algorithm is used in order to interpolate the solution among different chimera sub-grids, [8] [9] [10].

The introduction of propeller effects via viscous/inviscid coupling is obtained in a *body force* fashion. Specifically, propeller blades are not represented as solid boundaries of the computational domain and a cylindrical grid block is placed to fill the propeller region. Volume forces describing propeller induction and predicted by BEM, as shown later, are distributed over this grid block and added as source term $\mathbf{B}$ to the right-hand side of the momentum equations.

2.3 DES/BEM coupling

The viscous/inviscid coupling strategy in [15] is used here and briefly recalled for the sake of completeness. Viscous and inviscid-flow solutions are integrated through an interface in which two quantities are exchanged:

- volume-forces $\mathbf{B}$ recasting hydrodynamic forces on propeller blade surface by BEM as a volume force distribution in the Navier-Stokes equations;
- effective-inflow $\mathbf{w} = \mathbf{v} - \mathbf{v}_P$: rotational onset flow velocity to impose in BEM the impermeability condition on blades by using Eq. (2).

Volume forces **B** are derived by a time-accurate procedure that preserves spatial distribution and position in time of hydrodynamic forces exchanged between fluid and propeller blades.

At each time step, loading $(-p\mathbf{n} + \boldsymbol{\tau})$ (Eq. (4)) is pointwise averaged on blade suction and pressure sides and associated to the actual position of the blade mean surface $\hat{\mathcal{S}}_{B_k}$. The resulting force distribution is referred to a cylindrical coordinate system $(Oxr\theta)$, Fig. 1(a) and can be written as $\mathbf{b} = \mathbf{b}(x, r, \theta, t)$. By definition, **b** is zero at points (x, r, θ) outside $\hat{\mathcal{S}}_{B_k}$. Recalling that **b** represents a time-dependent Dirac distribution along coordinate x, an equivalent volume distribution can be easily obtained by introducing a function $\xi = \xi(x)$

$$\int \mathbf{b}(x, r, \theta, t)dx \; = \; \mathbf{b}_0(r, \theta, t) \int \xi(x)dx \tag{6}$$

In the present work, $\xi = \xi(x)$ is a normalised Gaussian distribution. For each value of r, θ, the function is centered at point x identifying the position of surface $\hat{\mathcal{S}}_{B_k}$ at time t. An example of the Gaussian distribution is shown in bottom right Fig. 2 below. The steepness of the Gaussian function controls the thickness in x direction of the region where volume forces replacing blade effects are imposed. In the present study, the distribution is chosen to have that the integral in the right-hand side of Eq. (6) is 0.99 when the integration interval along x equals 0.075 propeller diameters.

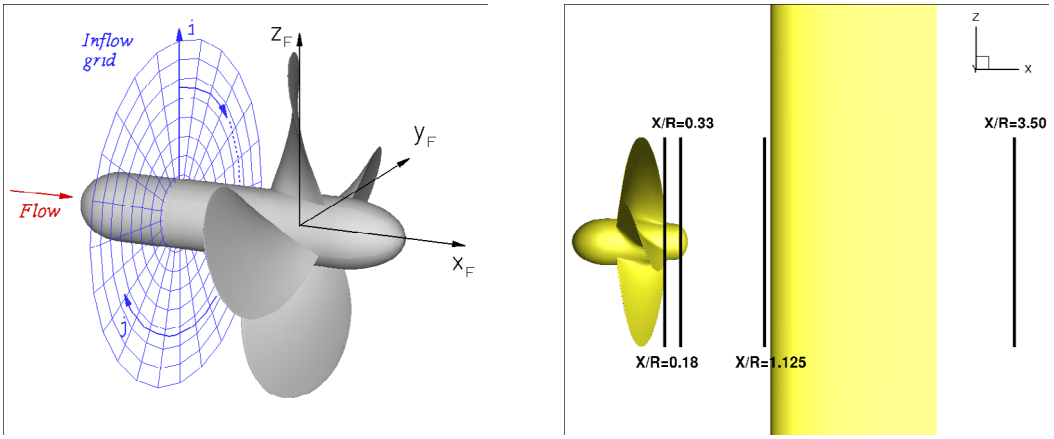

(a) Cylindrical coordinate system (x, θ, r) and Cartesian frame of reference $(Ox_F y_F z_F)$ used by BEM.

(b) Side view of the assembly with vertical planes downstream propeller and rudder.

Figure 1: Three-dimensional model of the propeller-rudder assembly.

The coupling between viscous and potential-flow solutions is achieved within the inner iteration of the dual–stepping procedure anticipated in section 2.2.

At the initial pseudo–time step, the viscous onset flow is obtained by the solution of Eqs. (5) with zero volume forces **B** describing propeller effects. The resulting velocity distribution **v** (which is not even a soleinodal field, as convergence in the inner iteration is not reached) is used to evaluate the inflow to the propeller as $\mathbf{w} = \mathbf{v}$. A first estimate of the propeller–induced perturbation is obtained by using **w** to impose boundary conditions by Eq. (2) and solve BEM equations, and a first guess of volume force distribution **B** follows.

From this point, the inner integration in the pseudo–time is started and convergence to a soleinodal field is reached together with convergence of the viscous–potential flow solutions.

We found that it is uselessly burdensome update **B** at each pseudo–time step, and that the best compromise was to call the BEM solver every $O(10)$ pseudo–time steps. In this way, every new estimation of **B** predicted by BEM is not too different from the previous one and the convergence of the inner iteration of the viscous solver is not hindered.

The unsteady-flow BEM solution is synchronised with propeller rotation in the viscous flow solution, except at the first time step, when the unsteady BEM solution is initialised by marching in time for a number of revolutions to achieve a correct description of transient flow contributions from the trailing wake, see Eq. (3).

As already mentioned, the BEM used here describes an isolated propeller, and hence no rudder surface contribution is explicitely given in Eq. (3). Presence of the rudder in the potential flow solution is accounted for through the effective inflow **w** where rudder perturbation to the flow field is described by the viscous flow solution of Eq. (5) with propeller perturbation included via source terms. An approximation in the evaluation of the effective inflow **w** is due to the fact that velocity contributions **v** and $\nabla\varphi$ are evaluated not on the actual propeller surface but over a plane perpendicular to the propeller axis corresponding to the upstream boundary of the volume force grid block.

3 NUMERICAL APPLICATION

A numerical application of the hybrid DES/BEM methodology is presented here by considering the interaction between a propeller and a rudder in its race under uniform onset flow conditions. Results by hybrid DES/BEM are validated against full-DES calculations using the methodology described in [11]. This study extends the analysis in [15], where an isolated propeller in uniform flow is addressed and hybrid unsteady RANSE/BEM results are compared with full-RANSE results. In both cases, the four-bladed INSEAN E779A model propeller, with diameter $D = 227.27$ mm is considered (see [13] for details).

A notional propeller-rudder assembly is analysed here in which the rudder is given by a straight cylinder with NACA 0020 sections aligned to the propeller axis and span extending to the farfield boundary of the computational domain. Rudder chord is $1.58R$ and leading edge is placed at distance $1.18R$ downstream the propeller plane. A sketch of the propeller-rudder assembly is given in Fig. 1(b).

Table 1 summarizes main geometry parameters and operating conditions considered in the numerical study. The Reynolds number is defined as $Re = \pi n D^2/2\nu$, by considering propeller radius $R = D/2$ as the reference length and velocity of blade tip as the reference speed, $V_{ref} = 2\pi n R$. The non-dimensional revolution period is then $T = 2\pi$. Considering inflow speed $V_0 = 5$ m/s and rotational speed $n = 25$ rps, propeller operates at advance coefficient $J = V_0/nD = 0.88$, that corresponds to the design point for the INSEAN E779A screw.

The computational domain for the numerical solution of the DES equations is delimited by a cylinder co-axial to propeller axis, with diameter of 50 D, axial length of 50 D and inlet/outlet planes at 25 D from the propeller plane. Full-DES computations are performed on three grid levels. The finest grid consists of 18.9M cells, with 2.4M discretizing the fluid domain surrounding blades, and coarser grids are obtained by removing every other point from the finer level. Using

Table 1: Propeller-rudder case study: geometry and operating conditions

INSEAN E779A propeller		Rudder	
Number of blades	4	Section	NACA0020
Diameter	0.227 m	Chord	0.18 m
Pitch ratio (0.7R)	1.183	Span	*infinite*
Expanded area ratio	0.468	Deflection angle	0 deg
Hub ratio	0.295	Distance LE-Prop. plane	0.134 m
Operating conditions			
Onset flow velocity, V_0	5 m/s	Reynolds number, Re	1.78×10^6
Propeller rate of revolution, n	25 rps	Advance coefficient, J	0.88

the hybrid DES/BEM model, the volume grid is the same of the full-DES case except for blade-fitted blocks replaced by the volume-force block. This yields a saving of 2.2M cells on the finest grid with respect to full-DES. Details of grid blocks surrounding the propeller and the rudder are shown in Fig. 2, where differences between grids used for full-DES (left) and for hybrid DES/BEM (right) are apparent. In particular, blade-fitted blocks necessary for capturing blade boundary layer in the full-DES analysis are replaced by a simple torus filling the volume spanned by rotating blades. For the inviscid-flow BEM solution, each blade surface is discretized into 864 elements and the hub surface into 624 elements. The trailing wake surface (see Eq. 3) extends for 3 revolutions with 3240 elements per revolution.

Both hybrid and full DES simulations are time-marching to describe the swirled flow induced by the rotating propeller to the rudder downstream. In full-DES calculations, propeller and hub blocks rotate with respect to fixed blocks built around rudder and background. Time stepping corresponds to 1 deg propeller rotation. In the hybrid DES/BEM simulation, the whole volume grid is fixed to the rudder and the hub surface is non-rotating. Only the surface grid used to discretize blades and hub in the BEM solution rotates, with time discretization of 2 deg per step.

Bottom right picture in Fig. 2 shows the volume force block and the distribution of volume force terms over a longitudinal axial plane. It may be noted that the inner boundary of the turus is not fitted to the tapered hub surface. As a consequence, there is a thin layer at blade root where no volume terms are defined to simulate the presence of the blade. The impact of differences between grids and boundary conditions at the hub is discussed in the following pages.

In order to compare results of numerical solutions by hybrid DES/BEM and by full DES, it is fundamental to verify that the hydrodynamic loading generated on propeller blades is consistent between the two solutions. Specifically, thrust T and torque Q obtained by integrating normal and tangent stress by BEM are to be compared with corresponding quantities from the full DES solution. In addition to this, thrust and torque obtained by integrating volume force terms are also to be verified to quantify possible errors related to recasting surface loads by BEM as volume loads. Transient loads using these different definitions are plotted in Fig. 3, while averaged values over a propeller revolution period are collected in Table 2. For the sake of completeness, thrust and torque contributions evaluated on the hub surface and axial force on the rudder F_x are also given. Recalling the rudder has a theoretically infinite span, in the present analysis loads are obtained by integrating over a surface with extension of 1.3 D and centered at propeller axis.

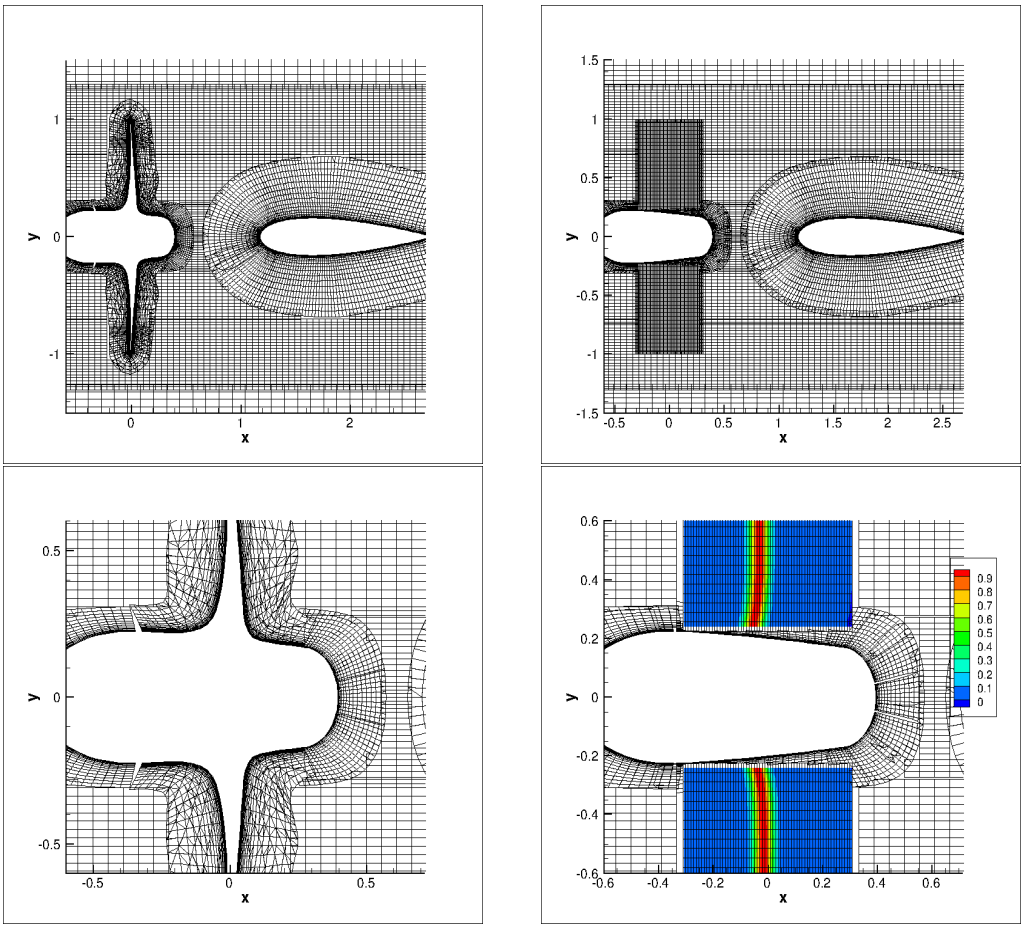

Figure 2: Discretization of the fluid region around propeller and rudder over a a horizontal plane at $z = 0$: full DES (left) and hybrid DES/BEM (right). Top: propeller and rudder. Bottom: details of grid blocks around the hub surface.

The following definitions of thrust, torque and axial force coefficients are used

$$K_T = \frac{T}{\frac{1}{2}\rho n^2 D^4}, \qquad K_Q = \frac{Q}{\frac{1}{2}\rho n^2 D^5}, \qquad K_{F_x} = \frac{F_x}{\frac{1}{2}\rho n^2 D^4}. \tag{7}$$

Left Fig. 3 shows that thrust and torque on blades obtained as volume force integral in the hybrid DES/BEM model overestimate full-DES predictions, with differences of time-averaged values of 6.8% for K_T and 4.9% for K_Q, see Table 2. Force fluctuations ΔK_T and ΔK_Q by hybrid DES/BEM are sensibly higher than those predicted by full DES. Volume forces are lower than surface loads by BEM, with negligible differences for thrust while torque reduces of 4.2%.

Axial forces on the hub surface and on the rudder portion are plotted in right Fig. 3. Differences between hybrid DES/BEM and full DES predictions of hub thrust are small but since averaged values are very small, a high percentual error of 70% is found. This can be explained recalling that, as discussed above, the hub region is where full DES and hybrid DES/BEM computational set-ups present main differences.

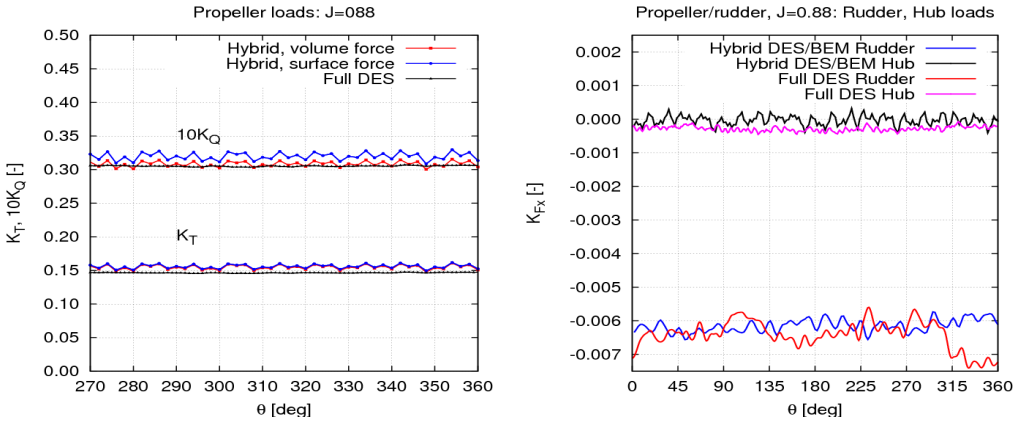

Figure 3: Time histories of propeller-rudder system loads, J=0.88. Left: thrust and torque on propeller blades. Right: axial force on rudder and hub.

In contrast to this, it is interesting to observe that time histories of axial force on the rudder evaluated by the two models are in fair agreement, with hybrid model result only 6.8% lower than DES. This can be considered as a global indicator that full DES and hybrid DES/BEM provide comparable descriptions of propeller induction to the flow field surrounding the rudder. A deeper analysis of this aspect is the objective of the present study and to this aim, velocity and pressure fields downstream the propeller are investigated.

Table 2: Propeller-rudder system loads, J=0.88. Time-averaged loads and fluctuations on propeller blades, hub and rudder.

Non-dim. loads	Full DES	Hybrid DES/BEM
Propeller (blades only)		
K_T (average)	0.146	0.156
$10K_Q$ (average)	0.305	0.320
$\Delta K_T/K_T$	2.1%	7.7%
$\Delta K_Q/K_Q$	1.3%	6.9%
Rudder		
K_{F_x} (average)	-6.59×10^{-3}	-6.14×10^{-3}
Hub		
K_T (average)	-1.22×10^{-4}	-0.35×10^{-4}
$10K_Q$ (average)	-2.33×10^{-4}	-0.53×10^{-4}

Axial velocity distributions on transversal planes downstream the propeller are shown in Fig. 4 at time step corresponding to blade in the reference position $\theta = 0$. Planes are located downstream the region swept by blade trailing edges ($x/R = 0.18$), upstream the rudder leading edge ($x/R = 1.125$), and downstream the rudder trailing edge ($x/R = 3.5$), Fig. 1(b). The black circle in bottom left Fig. 4 indicates the outer boundary of the volume force block.

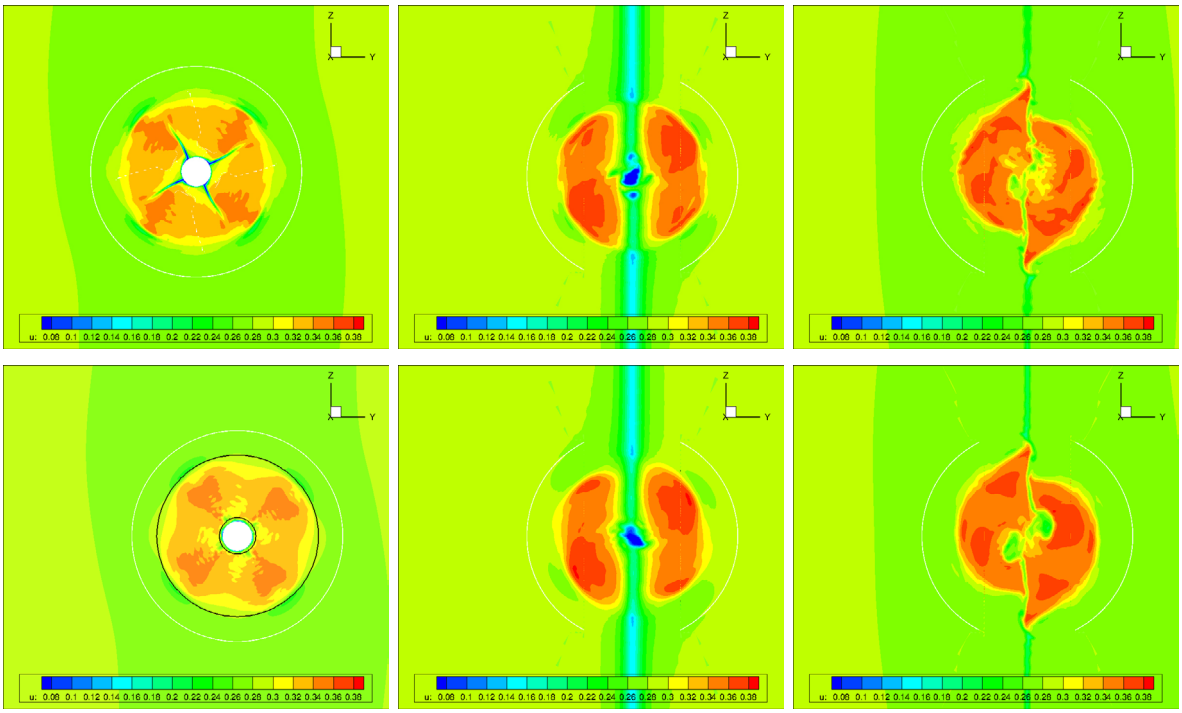

Figure 4: Contour map of axial velocity field at propeller angular position $\theta = 0°$ and vertical planes at (left to right) $x/R = 0.18, 1.125, 3, 5$. top: full DES; bottom: hybrid DES/BEM.

A qualitative comparison highlights a good agreement between results from the two approaches, with the solution based on propeller blades replaced by volume force terms inducing smoother distributions of axial velocity than the fully resolved solution. While such a trend is expected, it is interesting to observe that at plane $x/R = 1.125$ just downstream the volume force grid block, the hybrid model determines a velocity distribution that is consistent with the full DES solution. As expected for reasons discussed above, larger differences are observed in the hub region. Moving downstream, the agreement between hybrid DES/BEM and full DES solutions increases. In particular, the two solutions reveal the same mechanisms of interaction between propeller-induced flow and rudder surface. Vortical structures shed from blade tips and hub are splitted at the rudder leading edge in counter-rotating vortices. The resulting velocity field near the rudder surface yields to a composition of structures with the streamtube deformed and vertically shifted in opposite directions on starboard and portside. This is apparent on the plane downstream the rudder trailing edge (right Fig. 4), with distance between vortices tending to increase on the starboard side below the shaft and on the portside above the shaft. High velocity gradients are induced on the vertical midplane $y = 0$.

Quantitative comparisons of predicted velocity distributions are presented in Figs. 5 and 6, for three selected radial locations over the two planes downstream the propeller ($x/R = 0.33$) and rudder trailing edge ($x/R = 3.5$), Fig. 1(b). Distributions of the axial velocity and of the intensity of in-plane velocity are shown at distances from propeller axis $r/R = 0.24, 0.75, 1.0$. As expected, the largest discrepancy between solutions is found at sections near the hub.

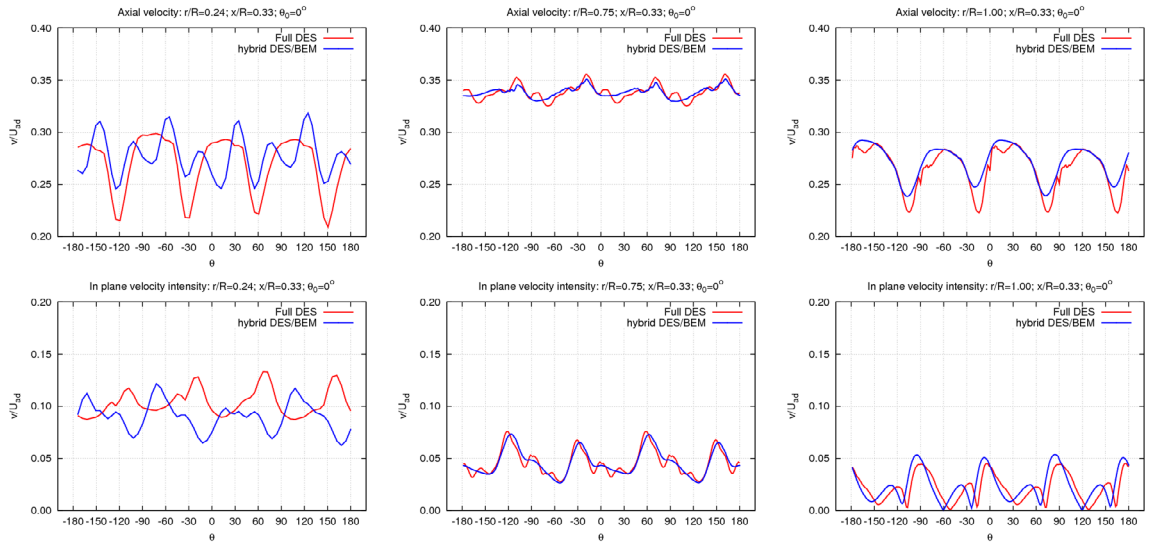

Figure 5: Velocity distributions on radial sections at transversal plane $x/R = 0.33$ and propeller position $\theta = 0°$. Left to right: $r/R = 0.24, 0.75, 1.0$. Top: axial velocity. Bottom: intensity of in-plane velocity.

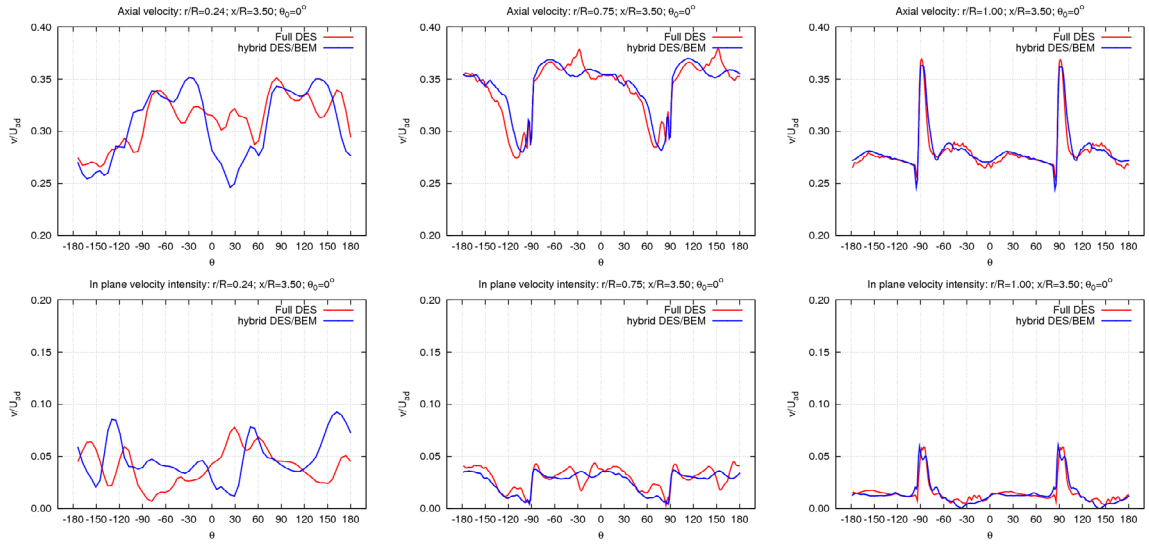

Figure 6: Velocity distributions on radial sections at transversal plane $x/R = 3.50$ and propeller position $\theta = 0°$. Left to write: $r/R = 0.24, 0.75, 1.0$. Top: axial velocity. Bottom: intensity of in-plane velocity.

The hub swirl effect is not taken into account in the hybrid approach and the propeller root representation by body forces is influenced by the thin gap between the tapered hub and the untapered volume force block, see Fig. 2. The agreement becomes good at outer radii just downstream the propeller (Fig. 5) and downstream the rudder (Fig. 6). Comparable velocity distributions are obtained both at $r/R = 0.75$ and at $r/R = 1.0$ where the effect of blade-shed

tip vortices dominates. As already noticed, velocity fluctuations are lower in hybrid DES/BEM results than in the full DES ones.

Further insight of flow field predictions are obtained by considering velocity distributions at vertical plane $y/R = 0.05$ and at horizontal plane $z = 0$. Contour maps of the axial velocity component are shown in Fig. 7. The black lines in the right pictures indicate upstream and downstream boundaries of the volume force block used by the hybrid model.

A limited agreement between results in the hub region is clearly shown, whereas the two solutions match very well in the other parts of the fluid domain and reveal the same flow features related to the propeller-shed wake and its interaction with the rudder. Different pressure distributions on rudder surface at starboard and portside influence the velocity distribution, with vortical structures impinging the rudder that are splitted and shed with different velocity on the two sides. This results into an asymmetric velocity distribution, here visible on vertical planes, top Fig. 7, that depends on the sense of rotation of the propeller. In the present case, with a right-handed screw, stronger axial velocity perturbation is found below the propeller axis line at starboard, while an opposite condition occurs at portside (not shown here), with stronger axial velocity perturbation above the propeller axis line.

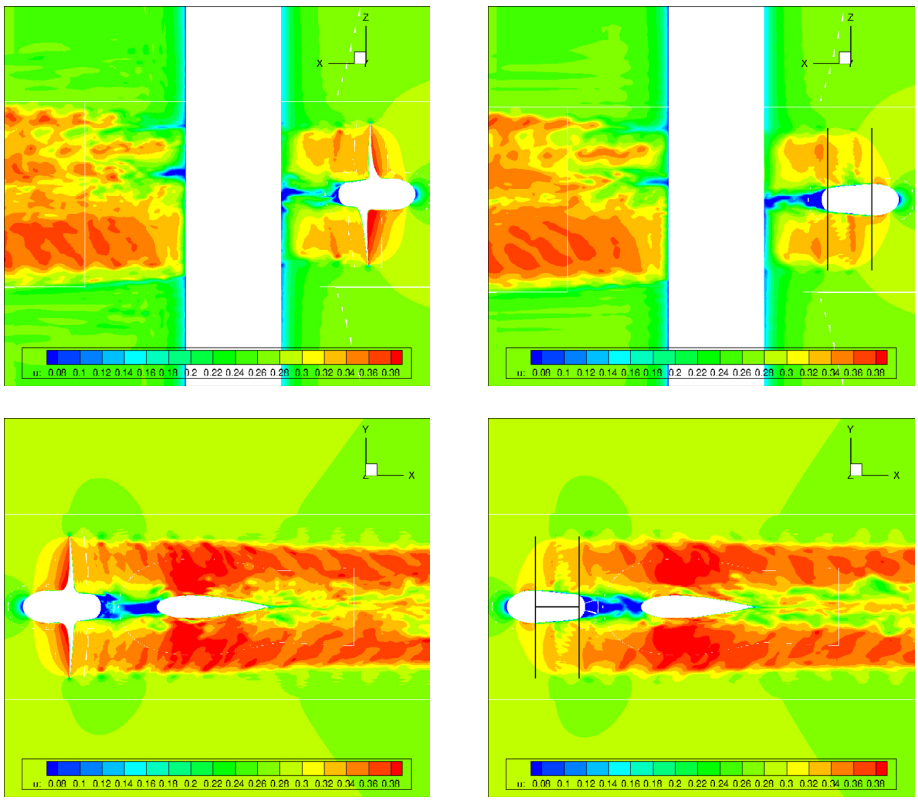

Figure 7: Contour map of the axial velocity field on longitudinal planes, propeller angular position $\theta = 0°$. Left: full DES. Right: hybrid DES/BEM. Top: vertical plane $y/R = 0.05$. Bottom: horizontal plane $z/R = 0$.

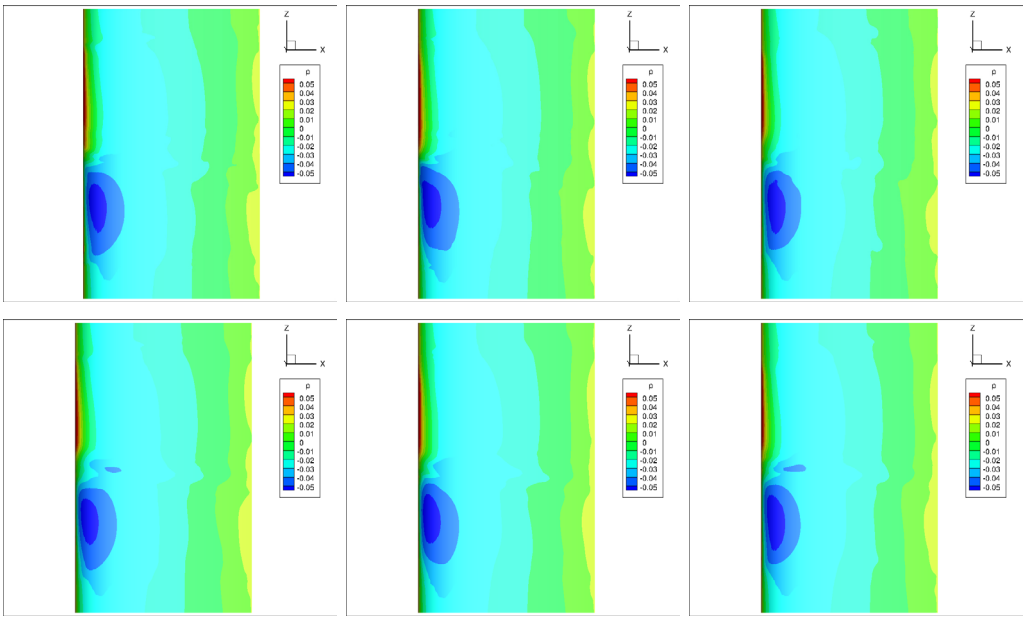

Figure 8: Contour map of rudder pressure distribution (portside) at propeller angular positions $\theta = 0, 30, 60$ deg. Top: full DES. Bottom: hybrid DES/BEM.

Pressure distributions on rudder portside for three time steps corresponding to blade angular positions $\theta = 0, 30, 60$ degrees are shown in Fig. 8. The agreement between hybrid DES/BEM and full DES solutions is very good, with fully comparable positive and negative pressure peaks in the leading edge region. This is confirmed by quantitative comparisons in Fig. 9 where chordwise pressure distributions on sections at $z/R = 0.75$ and 1.0 above the shaft line are plotted for a representative time step ($\theta = 0$). Small differences in predicted pressure distributions occur only in a narrow band where the hub vortex impinges the rudder leading edge. This may be detected in Fig. 8, and is quantified in Fig. 10 for a chordwise section at $z/R = 0.24$ above the shaft line and propeller positions $\theta = 0°$ and $90°$. Left and right plots in Fig. 10 refer to positions separated by 90 degrees that for the present four-bladed propeller corresponds to the blade passing period. It is interesting to observe that while the hybrid DES/BEM solution is nearly periodic with blade passing frequency, fluctuations are apparent in the full DES solution. Such a different behaviour can be explained with a general trend of the hybrid DES/BEM model to smooth out propeller-induced perturbations that can be captured when blades are actually described as solid boundaries.

Main findings from the present comparative analysis between hybrid DES/BEM and full DES solutions can be summarsed as follows:

- velocity fields predicted by the hybrid DES/BEM model are in agreement with those obtained from the full DES solution. This includes flow features like the trailing vorticity pattern in the propeller wake and its interaction with the rudder;
- a non-trivial result is that just downstream the fluid region where volume force terms are imposed to describe propeller induction, the solution by the hybrid DES/BEM model

agrees with the fully resolved DES solution;

- the hybrid DES/BEM model fails to capture high-frequency perturbations that are captured when blades are actually described as solid boundaries in the full DES solution.

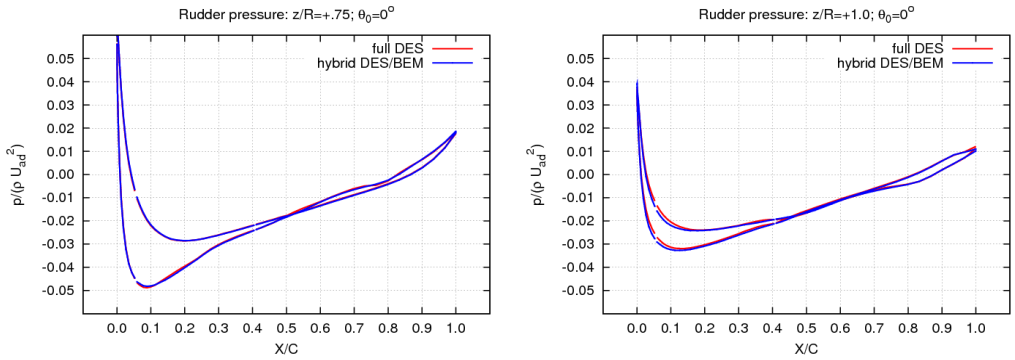

Figure 9: Chordwise pressure distribution on rudder sections $z/R = 0.75$ (left) and $z/R = 1.0$ (right). Propeller angular position $\theta = 0°$.

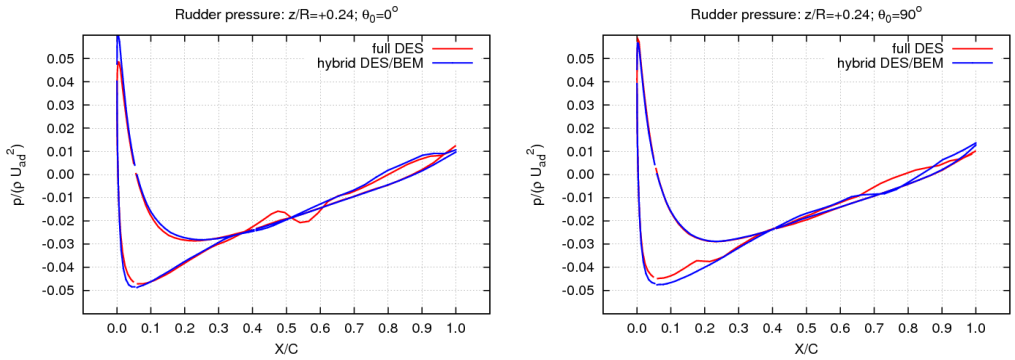

Figure 10: Chordwise pressure distribution on rudder section $z/R = 0.24$ at propeller angular positions $\theta = 0°$ (left) and $\theta = 90°$ (right).

4 CONCLUDING REMARKS

A generalised hybrid viscous/inviscid flow computational model for the simulation of propeller-induced flows has been presented and applied to the analysis of a propeller-rudder assembly. The methodology combines a Boundary Element Method (BEM) to predict propeller perturbation under inviscid-flow assumptions and a Detached Eddy Simulation (DES) Navier-Stokes solver to describe the viscous, turbulent flow around the rudder with propeller effects recast as volume-force terms from the BEM solution. The coupling between BEM and DES solvers is achieved via a time-marching iterative procedure to account for transient flow perturbation induced by a rotating propeller. The resulting computational model generalizes the concept of actuator disk used in ship hydrodynamics where only time averaged global propeller effects are described. The

model also generalizes existing hybrid RANSE/BEM models by coupling BEM with an unsteady DES Navier-Stokes solver to better describe transient turbulence and vorticity dynamics in the propeller wakefield.

Numerical results present hydrodynamic forces generated on propeller and rudder, pressure distributions on the rudder, velocity and vorticity downstream the propeller predicted by the hybrid DES/BEM model and validated by comparison with full DES solutions. Results of this validation study demonstrate the capability of the proposed hybrid viscous/inviscid flow model to reproduce full DES descriptions of propeller-induced perturbation to the rudder and the surrounding flow in spite of the fact that propeller blades are not resolved but simply described via volume forces by BEM. In particular, the analysis reveals a quantitative agreement between results from hybrid BEM/DES and full DES. Even at very small distance downstream the region where blades are replaced by volume forces, the hybrid model captures flow features with DES accuracy.

These findings may have a clear impact on applications of the proposed methodology to ship hydrodynamics problems where the transient flow perturbation induced by rotating propulsors is the objective of the study, as *e.g.*, to investigate propeller-rudder interaction, pressure pulse radiation to the hull plate, hydroacoustic noise emission, propeller action during manoeuvers. Numerical results from the present study show areas of further work necessary to improve the consistency of propeller force predicitions by the BEM model and to generalise the shape of the volume force block to fit tapered propeller hubs.

REFERENCES

[1] Calcagni, D., Salvatore, F., Muscari, R., Sundberg, J., Johansson, R. *Computational Analysis of Contra-Rotating Podded Propulsors Using a Hybrid RANSE/BEM Model*, 11^{th} Int. Conference on Hydrodynamics ICHD 2014, 19-24 October 2014, Singapore.

[2] Queutey, P., Deng, G.B., Guilmineau, E., Salvatore, F. *A comparison between full RANSE and coupled RANSE-BEM approaches in ship propulsion performance prediction.* 32nd Int. Conference on Ocean, Offshore and Artic Eng. (OMAE2013), Nantes, France, 2013.

[3] Di Mascio, A., Broglia, R., Muscari, R., and Dattola, R. *Unsteady RANS Simulation of a Manoeuvring Ship Hull*, 25^{th} Symposium on Naval Hydrodynamics ONR 2004, St. Johns, Newfoundland, Canada, 8-13 August 2004.

[4] Hally, D. *Propeller Analysis Using RANS/BEM Coupling Accounting for Blade Blockage*, IV^{th} Int. Symposium on Marine Propulsors SMP'15, June 2015, Austin, Texas, USA.

[5] Kerwin, J.E., Keenan, D.P., Black, S.D., Diggs, J.G. A Coupled Viscous/Potential Flow Design Method for Wake-Adapted, Multi-Stage, Ducted Propulsors Using Generalized Geometry. *SNAME Transactions* (1994) **102**:23-56.

[6] Merkle, C.L., Athvale, M. *Time-accurate Unsteady Compressible Flow Algorithms Based on Artificial Compressibility.* AIAA Paper 87-1137, 1987.

[7] Morino, L. Boundary Integral Equations in Aerodynamics, *Applied Mechanics Reviews* (1993) **46**(8):445-466.

[8] Muscari, R. and Di Mascio, A. *Simulation of the flow around complex hull geometries by an overlapping grid approach*, Proc. 5^{th} Osaka Colloquium on advanced research on ship viscous flow and hull form design by EFD and CFD approaches, Osaka, Japan, March 2005.

[9] Muscari, R., Broglia, R., and Di Mascio, A. *An overlapping grids approach for moving bodies problems*, 16^{th} Int. Offshore and Polar Engineering Conference ISOPE 2006, San Francisco, California, USA.

[10] Muscari, R., Felli, M., and Di Mascio, A. Analysis of the Flow Past a Fully Appended Hull with Propellers by Computational and Experimental Fluid Dynamics, *ASME Journal of Fluids Engineering* (2011), **133**(6):61-104.

[11] Muscari, R., Dubbioso, G. and Di Mascio, A. Analysis of the flow field around a rudder in the wake of a simplified marine propeller, *Journal of Fluid Mechanics* (2017) **814**:547-569.

[12] Rijpkema, D., Starke, B., Bosschers, J. *Numerical simulation of propeller-hull interaction and determination of the effective wake field using a hybrid RANS-BEM approach*, III^{rd} Int. Symposium on Marine Propulsors SMP'13, May 2013, Launceston, Tasmania.

[13] Salvatore, F., Alves Pereira, F., Felli, M., Calcagni, D., Di Felice, F. *Description of the INSEAN E779A Propeller Experimental Dataset,* INSEAN Technical Report 2006-085, INSEAN, Rome, Italy, 2006.

[14] Salvatore, F., Greco, L., Calcagni, D. *Computational analysis of marine propeller performance and cavitation by using an inviscid-flow BEM model*, 2^{nd} Int. Symposium on Marine Propulsors, SMP'11, Hamburg, Germany, 15-17 June 2011.

[15] Salvatore, F., Calcagni, D., Muscari, R., Broglia, R. *A generalised fully unsteady hybrid RANS/BEM model for marine propeller flow simulations*, VI^{th} Int. Conference on Computational Methods in Marine Engineering MARINE 2015, 15-17^{th} May 2015, Rome, Italy, Francesco Salvatore, Riccardo Broglia and Roberto Muscari (Eds.), pp. 613-626.

[16] Sanchez-Caja, A., Martio, J., Saisto, I., and Siikonen, T. On the enhancement of coupling potential flow models to RANS solvers for the prediction of propeller effective wakes. *Journal of Marine Science and Technology* (2014) **20**(1):104-117.

[17] Spalart, P.R. Detached-Eddy Simulation, *Annual Review of Fluid Mechanics* (2009) **41**:181-202.

[18] Sparenberg, A. On the potential theory of the interaction of an actuator disc and a body, *Journal of Ship Research* (1972) **16**:271-277.

[19] Wockner, K., Greve, M., Scharf, M., Abdel-Maksoud, M. *Unsteady Viscous/Unviscid Coupling Approaches for Propeller Flow Simulations*, 2^{nd} Int. Symposium on Marine Propulsors, SMP'11, Hamburg, Germany, 15-17 June 2011.

[20] Zhang, D.H. Numerical Computation of Ship Stern/Propeller Flow, Doctoral Thesis, *Chalmers University of Technology*, Gothenburg, Sweden, (1990).